Title: Climate explains geographic and temporal variation in mosquito-borne disease dynamics on two continents

Jamie M. Caldwell[1], A. Desiree LaBeaud[2], Eric F. Lambin[3,4], Anna M. Stewart-Ibarra[5,6], Bryson A. Ndenga[7], Francis M. Mutuku[8], Amy R. Krystosik[2], Efraín Beltrán Ayala[9], Assaf Anyamba[10], Mercy J. Borbor-Cordova[11], Richard Damoah[12], Elysse N. Grossi-Soyster[2], Froilán Heras Heras[13], Harun N. Ngugi[14,15], Sadie J. Ryan[16-18], Melisa M. Shah[19], Rachel Sippy[13,20,21], Erin A. Mordecai[1]

[1] Department of Biology, Stanford University, 371 Serra Mall, Stanford, California, USA

[2] Department of Pediatrics, Division of Infectious Diseases, Stanford University, 300 Pasteur Drive, Stanford, California, USA

[3] School of Earth, Energy & Environmental Sciences, and Woods Institute for the Environment, Stanford University, Stanford, California 94305, USA.

[4] Georges Lemaître Earth and Climate Research Centre, Earth and Life Institute, Université catholique de Louvain, 1348 Louvain-la-Neuve, Belgium.

[5] Department of Medicine and Department of Public Health and Preventative Medicine, SUNY Upstate Medical University, Syracuse, NY, USA

[6] InterAmerican Institute for Global Change Research (IAI), Montevideo, Uruguay

[7] Centre for Global Health Research, Kenya Medical Research Institute, Kisumu, Kenya

[8] Department of environment and health sciences, Technical University of Mombasa, Mombasa, Kenya

[9] Technical University of Machala, Machala, Ecuador

[10] Universities Space Research Association and NASA Goddard Space Flight Center, Greenbelt, MD, USA.

[11] Facultad de Ingeniería Marítima y Ciencias del Mar, Escuela Superior Politécnica del Litoral, ESPOL, Guayaquil, Ecuador

[12] Morgan State University and NASA Goddard Space Flight Center, Greenbelt, MD, USA.

[13] Center for Research SUNY-Upstate-Teófilo Dávila Hospital, Machala, Ecuador

[14] Department of Biological Sciences, Chuka University, Chuka, Kenya

[15] Department of Zoology, School of Biological Sciences University of Nairobi, Nairobi, Kenya

[16] Emerging Pathogens Institute, University of Florida, Gainesville, Florida

[17] Quantitative Disease Ecology and Conservation (QDEC) Lab, Department of Geography, University of Florida, Gainesville, Florida;

[18] School of Life Sciences, University of KwaZulu, Natal, South Africa

[19] Department of Medicine, Division of Infectious Diseases, Stanford University, 300 Pasteur Drive, Stanford, California, USA

[20] Institute for Global Health and Translational Science, SUNY-Upstate Medical University, Syracuse, NY, USA

[21] Department of Medical Geography, University of Florida, Gainesville, FL, USA

Abstract:

Climate drives population dynamics, but when the underlying mechanisms are unresolved, studies can lead to seemingly contradictory effects of climate on natural populations. Climate-sensitive vector-borne diseases such as dengue, chikungunya, and Zika are one example where climate appears to have opposing effects in different contexts. In this study, we use a mathematical model to directly connect climate-driven mosquito physiology measured in laboratory studies to observed vector and disease dynamics in the field across ecologically and culturally distinct settings in Ecuador and Kenya. We show that temperature, rainfall, and humidity predict *Aedes aepgyti* abundances and laboratory-confirmed arboviral incidence across ecologically distinct settings. Further, this trait-based approach resolves seemingly contradictory results from prior field studies and highlights climate conditions where mechanisms remain unresolved. Using this mechanistic model, we tested several intervention strategies and found that reducing immature mosquito habitat or contact rate between mosquitoes and humans are more effective interventions than killing adult mosquitoes. These results can help guide intervention efforts and improve climate change predictions for vector-borne diseases.

Introduction:

Climate is a major driver of species interactions and population dynamics, but the mechanisms underlying these relationships are often poorly understood and rarely tested in the field [1]. One of the primary ways that climate impacts populations is through its effects on species' vital rates [2]. However, these mechanistic effects can lead to

seemingly contradictory results in the field because multiple climate variables may act synergistically, with each climate variable potentially affecting multiple vital rates, and their impacts may be nonlinear, changing direction and relative importance across a gradient of conditions. Vector-borne diseases provide an interesting case study to test whether climate sensitive traits measured in controlled, laboratory settings can reconcile seemingly contradictory results from field studies. For example, mosquito-borne arboviral diseases such as dengue, chikungunya, and Zika are clearly climate-sensitive: a body of field research has consistently identified temperature, rainfall, and humidity as important predictors of disease, but sometimes with opposite conclusions about the magnitude and direction of effects of climate on mosquito and disease dynamics [3–8]. For example, dengue incidence correlated with temperature positively in Mexico [9] but negatively in Thailand [10]. We hypothesize that such opposing effects could be simultaneously correct if disease dynamics are context-dependent or nonlinear, and each model describes true disease dynamics but only within a small subset of conditions (e.g., specific locations or seasons).

Understanding the mechanisms that drive disease dynamics is particularly important for arboviruses like dengue, chikungunya, and Zika because they are a major public health burden, vector control is the main method for breaking transmission cycles, and the burden and distribution of these diseases are projected to shift geographically in the future [11–13]. Half of the world's population is currently at risk of contracting dengue [14]. With no widely available vaccine, vector control remains the primary method for preventing arboviral disease transmission. Existing vector control methods focus on

93 reducing immature habitat, reducing adult populations, or employing personal protection
94 to reduce contact between infected mosquitoes and people [15]. Like other vector-borne
95 diseases with complex transmission dynamics, model simulations can help guide
96 effective intervention efforts [16,17]. Further, mechanistic models are better suited to
97 predict how climate change will impact future disease burden and distribution, as
98 projected climate conditions are outside the current arboviral climate niche space.
99
100 Dengue, chikungunya, and Zika are climate-sensitive diseases because of the ecology of
101 *Aedes aegypti*, the primary disease vector. *Ae. aegypti* are anthropophilic, globally
102 distributed mosquitoes that breed in artificial containers with standing water [18,19]. All
103 mosquito and parasite traits that are important for transmission and linked to metabolism,
104 such as reproduction, development, survival, biting rate, and extrinsic incubation period,
105 are temperature dependent with a thermal optima [20–22]. Humidity is positively
106 associated with mosquito survival because the high surface area to volume ratio of
107 mosquitoes exposes them to desiccation [23,24]. Standing water from rainfall provides
108 essential larval and pupal habitat for mosquitoes, but the relationship is complex because
109 heavy rainfall can flush away breeding habitats [25–27] and water storage practices
110 during droughts can increase water availability, mosquito abundance, and contact
111 between mosquitoes and people [28–30].
112
113 In this study, our goal was to test the extent to which climate-driven mosquito traits drive
114 disease dynamics across two geographically distinct regions and to characterize the
115 effectiveness of different intervention strategies in those regions. Specifically, we asked:

116 1) how accurately do mechanistic model predictions reproduce observed mosquito and
117 disease dynamics in the field, 2) are there conditions where the model systematically fails
118 to reproduce observed disease dynamics, and 3) what is the relative effectiveness of
119 different intervention strategies given different levels of intervention effort? To answer
120 these questions, we adapted a mechanistic model for arboviral transmission as a function
121 of climate and independently validated the models with data collected on *Ae. aegypti*
122 abundances and laboratory-confirmed dengue, chikungunya, and Zika cases from two
123 equatorial countries with distinct socioeconomic, geographic, cultural, and disease
124 transmission settings: Ecuador and Kenya (Fig. 1, Table S1). The study sites within each
125 country were distributed across a temperature gradient with similar ranges of humidity
126 and rainfall. Previous studies have found that *Ae. aegypti* and dengue were positively
127 associated with warm and wet conditions in Ecuador and Kenya [31–34], although other
128 *Ae. aegpyti*-vectored arboviruses in Kenya such as chikungunya have been associated
129 with warm and dry conditions [35]. In addition to similar climate conditions, both
130 countries have hyperendemic transmission of all four dengue serotypes and have recently
131 experienced outbreaks of chikungunya; yet, arboviral transmission dynamics differ in
132 each country. In Ecuador, dengue is a re-emerging disease with large seasonal epidemics
133 that frequently result in severe dengue [31]; by contrast, in Kenya, dengue has low levels
134 of year-round transmission [36] and intermittent self-limiting outbreaks that are often
135 undetected [37]. Further, compared with South America, sub-Saharan Africa lacks severe
136 dengue, perhaps because African strains of *Ae. aegpyti* have lower susceptibility to all
137 four dengue serotypes [38], and/or because people of African ancestry are less
138 susceptible to severe dengue [39].

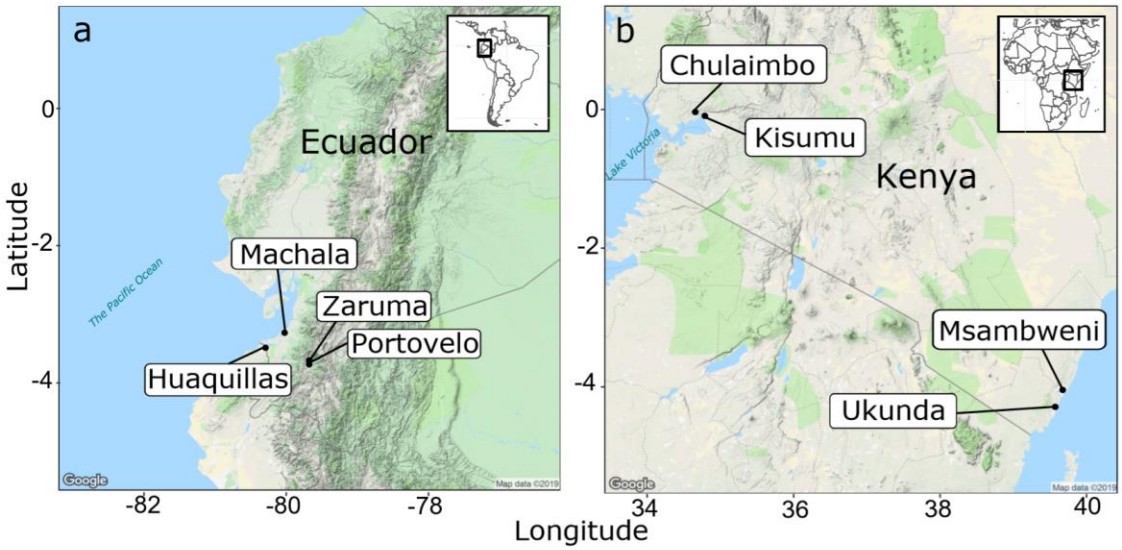

Figure 1: Study sites with distinct socioeconomic, geographic, cultural, and disease transmission settings. Study sites within a) Ecuador in South America and b) Kenya in East Africa. See Table S1 for additional site characteristics.

Results:

Relationship between model predictions and observed disease dynamics

The dynamic susceptible, exposed, infectious – susceptible, exposed, infectious, removed (SEI-SEIR) compartmental model (Fig. 2) parameterized with temperature-, rainfall-, and humidity-dependent mosquito life history traits was strongly associated with mosquito abundances and disease dynamics across sites and through time. Model-predicted mosquito abundances and field-collected observations of mosquito abundances corresponded with each other in 65% of the surveys (sample size N = 277 site-months) (Table 1), based on whether the z-scores of predictions and observations were within one standard deviation of each other. Based on surveys conducted across all vector life stages in Kenya (only adult mosquitoes were collected in the Ecuador surveys), the SEI-SEIR

155 model had similar correspondence with the abundance of adult mosquitoes (60%, N =
156 217) to pupae (60%, N = 217), late instars (57%, N = 217), early instars (56%, N = 217),
157 and eggs (50%, N = 216), likely because the dynamics were consistent across life stages.
158 Model-predicted disease cases corresponded with laboratory-confirmed arboviral
159 incidence in 83% of the surveys (N = 388 site-months) (Table 1). We used z-scores for
160 comparison because the model predictions represent total population estimates whereas
161 observations come from sub-samples of the mosquito and human population.
162

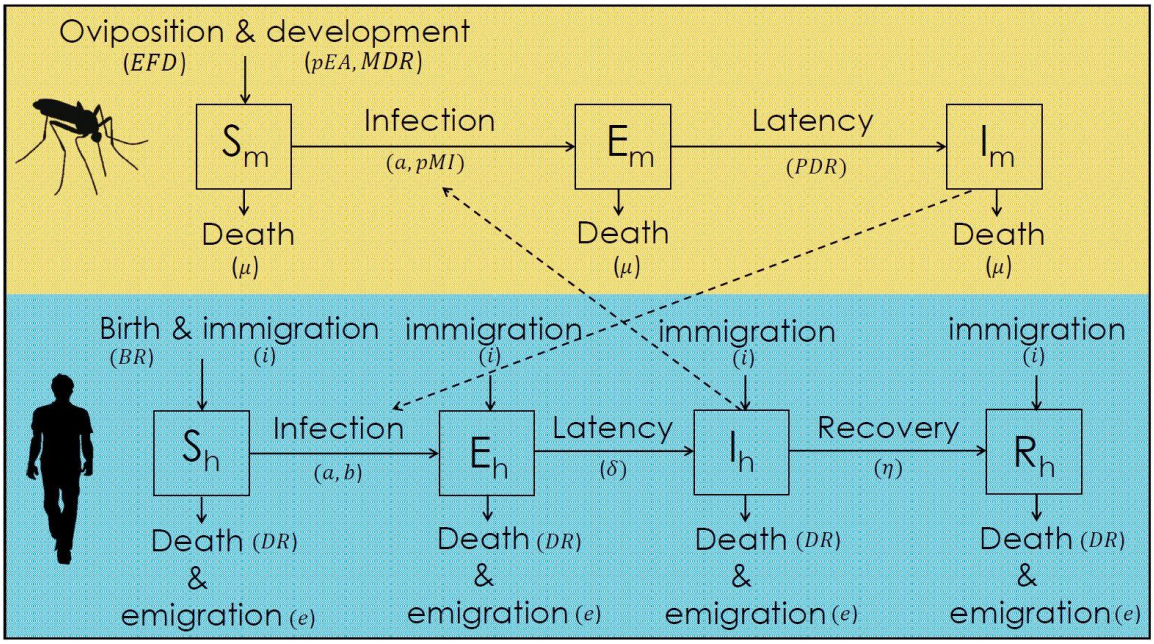

163

164 **Figure 2: SEI-SEIR epidemiological model framework.** The mosquito population (top
165 panel, orange) is split among susceptible (S_m), exposed (E_m), and infectious (I_m)
166 compartments (squares) and the human population (bottom panel, blue) is split among
167 susceptible (S_h), exposed (E_h), infectious (I_h), and recovered (R_h) compartments. Solid
168 arrows indicate the direction individuals can move between classes and dashed arrows
169 indicate the direction of transmission. Transitions among compartments are labeled by

the appropriate processes and corresponding rate parameters (see Methods for more detail).

Table 1: Model accurately predicted mosquito abundances and arboviral cases for majority of surveys. Rows correspond to comparisons between model predictions and field observations for mosquito abundances or arboviral cases. Correspondence indicates that z-scores of model predictions and field observations fell within one standard deviation of each other. Overprediction indicates that the z-score of the model predictions were more than one standard deviation above the z-score of the observations, and vice versa for underprediction. The percent of total surveys are presented in parentheses beside the total number of surveys (N) in each category. Table S2 shows the same data separated by site.

Comparison	Correspondence	Overprediction	Underprediction	N
Mosquitoes	179 (65%)	52 (19%)	46 (16%)	277
Arboviral cases	322 (83%)	30 (8%)	36 (9%)	388

We explored three additional aspects of model fit and found that the model predicted the magnitude of observations moderately well and detected trends through time and differences across sites. Model-predicted mosquito abundances were positively correlated with field-collected observations of mosquito abundances (Pearson's correlation coefficient $r = 0.35$, sample size $N = 277$) (Fig. 3) and predictions and observations synchronously increased and decreased through time within sites (Exact two-tailed sign test, $p < 0.05$), but the annual proportion of observations predicted by the model differed across sites ($F(7,24) = 10.75$, $p < 0.001$). Similarly, model-predicted disease cases

192 correlated positively with laboratory-confirmed arboviral incidence (r = 0.19, N = 388)
193 (Fig. 3) and predictions and observations synchronously increased and decreased through
194 time within sites (Exact two-tailed sign test, $p < 0.001$), but the annual proportion of
195 observations predicted by the model differed across sites ($F(7,18) = 358.8$, $p < 0.001$).
196 Chikungunya and Zika incidence were only confirmed in Huaquillas and Machala,
197 Ecuador ($N_{dengue} = 366$, $N_{chikungunya} = 35$, $N_{Zika} = 14$); in those sites, arboviral incidence for
198 each disease peaked at different times and corresponded better with model predictions
199 than dengue alone (Fig. 4).
200

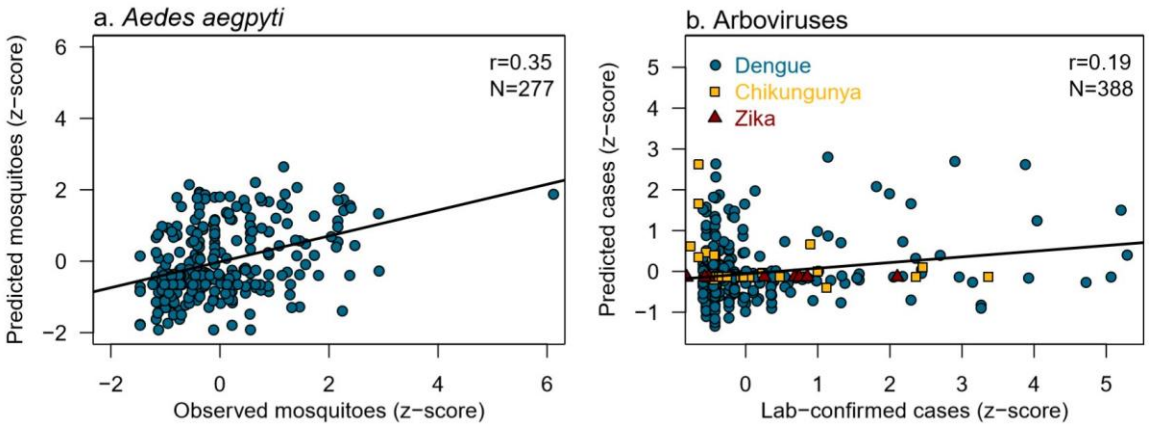

201

202 **Figure 3: The SEI-SEIR model positively correlated with field observations of**
203 **mosquito abundances and arboviral cases across all sites.** a) Scatterplot of the z-score
204 of the total modeled mosquito population versus the z-score of the mean number of adult
205 *Ae. aegypti* trapped per house, across sites and months between 2014 and 2018. b)
206 Scatterplot of the z-score of predicted disease cases in the human population versus the z-
207 score of laboratory-confirmed dengue, chikungunya, and Zika cases, across sites and
208 months between 2014 and 2018. The solid black lines are regression lines. Pearson's

209 correlation coefficient, r, based on the raw data, and the sample size, N, are presented in
210 the top right corner of the plots.
211

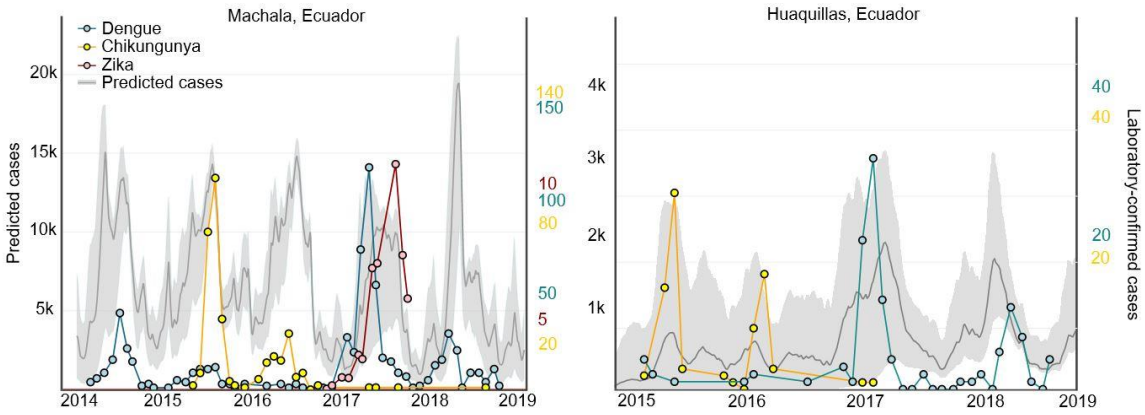

212

213 **Figure 4: Model-predicted disease cases reproduced general patterns of arboviral**
214 **transmission.** Solid grey line and shaded grey region shows median and 95% confidence
215 interval for model-predicted disease cases, blue dots and lines show laboratory-confirmed
216 dengue cases, yellow dots and lines show laboratory-confirmed chikungunya cases, and
217 red dots and lines show laboratory-confirmed Zika cases (note that the y-axes scales
218 differ for the three diseases). The 95% confidence intervals are based on 50 model
219 simulations using different c, T_0, and T_{max} estimates (see Methods) for temperature-
220 dependent traits from the posterior distributions found in [20].
221

222 We tested three hypothesized functional relationships between rainfall and mosquito
223 carrying capacity in the SEI-SEIR model (Fig. S1) and found that the rainfall function
224 that correlated most strongly with field observations differed by response variable
225 (mosquito abundance and arboviral incidence) and site (Table 2). We used correlation to
226 determine the best rainfall function because correlation is the most sensitive metric for

magnitude and the rainfall function in the model affects the magnitude of mosquitoes via carrying capacity. The model with the left-skewed unimodal (Brière) rainfall function (Fig. S1a), which indicates that mosquito abundances increase with increasing rainfall until some threshold where flushing occurs, described observed mosquito and disease dynamics most often (Table 2).

Table 2: Rainfall differentially affects mosquito and disease dynamics across sites. Each row corresponds to a study site and indicates the rainfall function that correlated most strongly with field observations of *Ae. aegpyti* abundances and arboviral cases, and the associated Pearson's correlation coefficient. The left-skewed unimodal Brière rainfall function (Fig. S1a) indicates that mosquito abundances increase with increasing rainfall until some threshold where flushing occurs. The symmetric unimodal quadratic rainfall function (Fig. S1b) indicates that mosquito abundances peak with intermediate amounts of rainfall and are reduced with low and high rainfall values. The exponentially decreasing inverse rain function (Fig. S1c) indicates that mosquito abundances peak when there is no or low rainfall, likely as a result of water storage practices. All measures of model fit (i.e., correspondence, correlation, sign tests, and ANOVAs) were based on models where the different rainfall functions listed in this table were used.

		Aedes aegpyti		Arboviruses	
Country	Site	Rain function	Correlation	Rain function	Correlation
Ecuador	Huaquillas	Brière	0.36	Inverse	0.63
Ecuador	Machala	Quadratic	0.63	Brière	0.12
Ecuador	Portovelo	Brière	0.66	Brière	0.07
Ecuador	Zaruma	Brière	0.41	Brière	0.30
Kenya	Chulaimbo	Brière	0.21	Quadratic	0.02
Kenya	Kisumu	Brière	0.50	Brière	0.25
Kenya	Msambweni	Inverse	0.28	Quadratic	0.28
Kenya	Ukunda	Brière	0.31	Inverse	0.07

Identifying conditions that systematically lead to divergence between predictions and observations

To determine if climate-based, geographical, and urbanization factors could explain conditions where the models consistently over- or underpredicted mosquito abundances and arboviral cases (Table 1), we used classification and regression tree (CART) models. We found that the model systematically overpredicted mosquito abundances when there was low to moderate rainfall (<55 mm) and moderate to high humidity (>1.2 kPA) (Fig. 5a). The model systematically overpredicted arboviral cases when there was high mean temperature (>29°C) or high minimum temperature (>24°C) (Fig. 5b). We did not find evidence of any conditions that systematically led to underpredicting mosquito abundances or arboviral cases, likely because there were many predicted and observed zeros. The 29°C breakpoint that we identified for arboviral cases aligns with the point at which the model predicts that the relative basic reproductive number (R_0) declines (Fig. 6). However, the CART results suggest that temperature-dependent mosquito traits may be more constrained at high temperatures than previously estimated from laboratory studies, potentially because of daily temperature variation. Previous field studies estimating the effects of temperature on dengue transmission further support this finding where, in general, locations with mean temperature below 29°C show a positive relationship with dengue incidence whereas locations with mean temperatures above 29°C show negative relationships (Fig. 6).

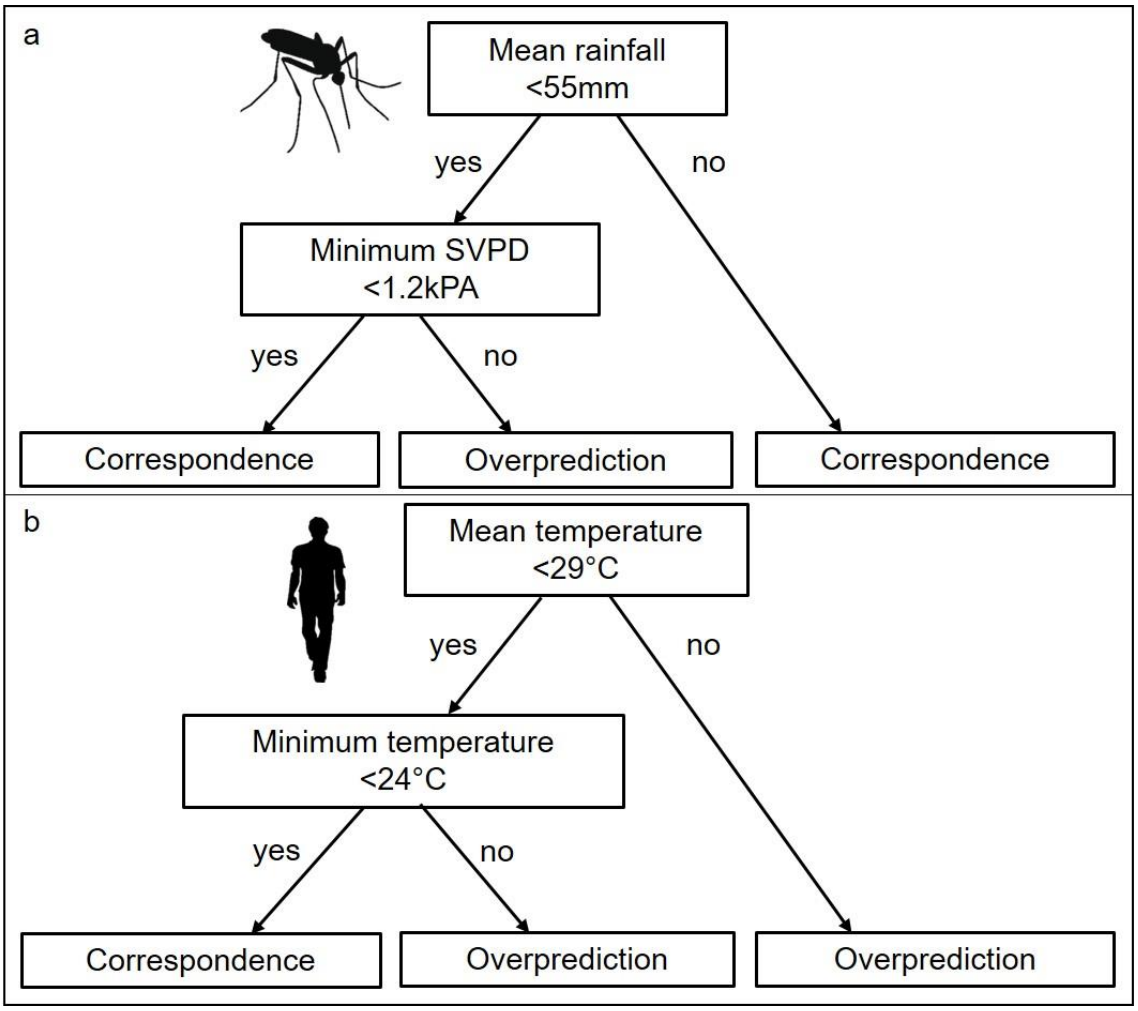

Figure 5: High rainfall, humidity, and temperature were associated with the model systematically overpredicting mosquito abundances and arboviral cases.

Classification and regression trees for a) mosquito abundances and b) arboviral cases. Climate conditions represent values within the month prior to a survey. The Saturation Vapor Pressure Deficit (SVPD) is a measure of humidity (see Methods).

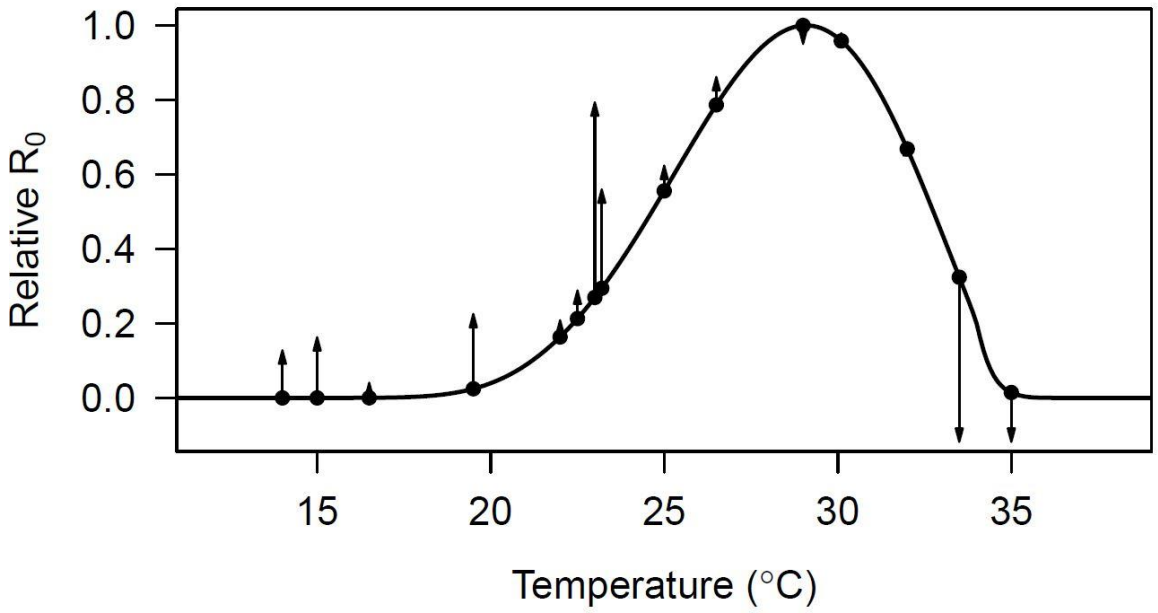

Figure 6: Independently predicted relative R_0 from an empirically derived model explains differences in the magnitude and direction of the effects of temperature on dengue transmission across varied settings from previous field studies. The black line shows the relative basic reproductive number (R_0, normalized to a 0-1 scale) plotted against temperature based on all temperature-dependent traits from [20] used in the SEI-SEIR model. Points indicate mean temperature values from previous field-based statistical analyses that related dengue cases with minimum, maximum, or mean ambient temperature; arrows correspond to the direction (up = positive, down = negative) and relative effect size of the temperature-dengue relationship based on coefficient values from studies in Bangladesh, China, Colombia, Guadeloupe, Mexico, Taiwan, Thailand, and Vietnam [9,10,40–49]. See Methods and Table S3 for more detail. As expected, the largest observed positive effects of temperature occurred in the rapidly increasing portion of R_0 curve (~22-25°C) and the largest observed negative effects occurred well above the predicted optimum, near the upper thermal limit (~33-35°C).

290 ***Evaluating the effectiveness of different intervention scenarios***

291 We simulated three intervention strategies at three intensity levels and found that
292 reducing immature mosquito habitat or contact rate between mosquitoes and humans are
293 far more effective intervention strategies than reducing adult mosquito abundance (Fig.
294 7). Even with high intensity intervention efforts that reduce mosquito abundance by 90%
295 (e.g., spraying large amounts of insecticide), the model indicates that we would expect
296 only 11% fewer human disease cases (Fig. 7; approximately 12 disease cases per 100,000
297 population). By contrast, a 10% reduction in immature mosquito habitat (e.g., removing
298 containers from the environment that create pools of standing water from rain) or contact
299 rate (e.g., using window screens, mosquito repellent, or wearing protective clothing)
300 would decrease disease cases by approximately 16% and 19%, respectively (Fig. 7;
301 approximately 110 and 187 disease cases per 100,000 population, respectively). Higher
302 intensity efforts that reduce immature mosquito habitat or contact rate by 50% or 90%
303 provides even greater protection, resulting in predicted decreases in disease cases by as
304 much as 96% (Fig. 7; approximately 2,087 disease cases per 100,000 population).

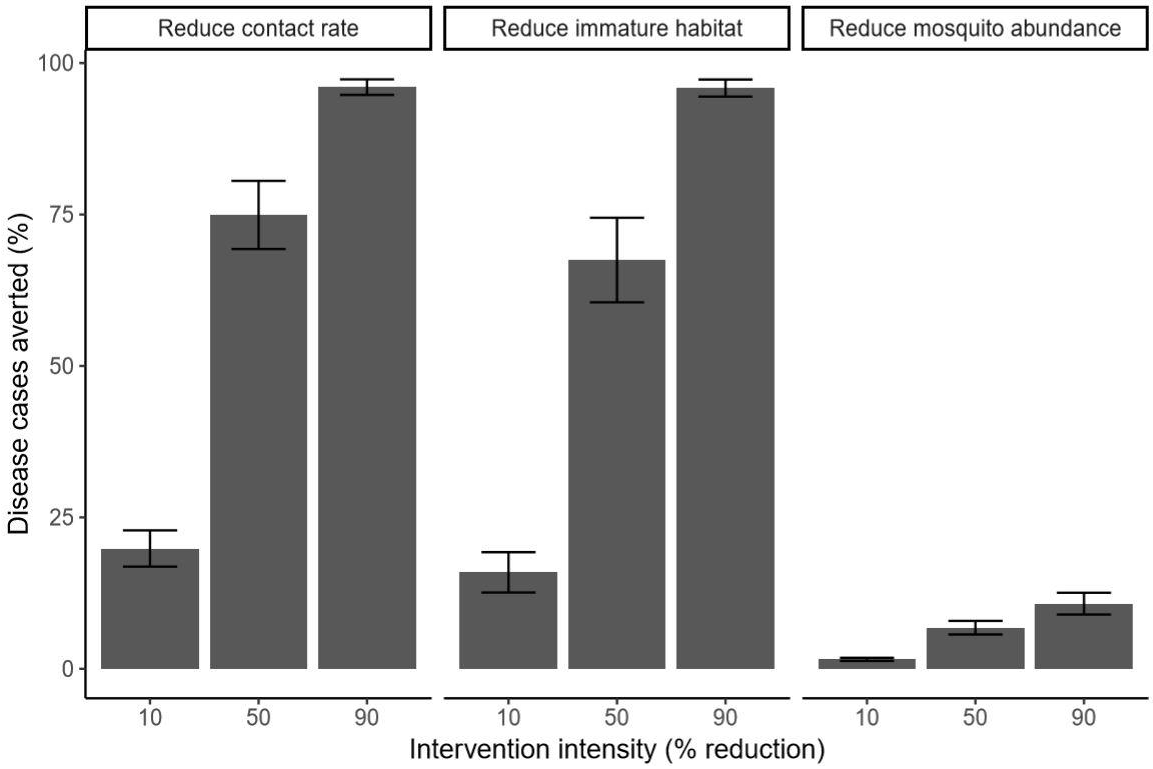

Figure 7: Reducing contact rate or immature mosquito habitat leads to the largest reductions in disease cases. Barplots show the predicted decrease in arboviral cases across three intervention strategies (reduce contact rate, reduce immature mosquito habitat, reduce mosquito abundance) and three intervention intensities (10%, 50%, and 90% reductions). Bars indicate the mean across study sites of the difference between the number of predicted disease cases in a population (e.g., number of cases at one site over a one-year time period) and the number of predicted disease cases in the same population and time period given a specific intervention strategy at a specific intensity level). The error bars indicate the standard error of the mean across all eight study sites.

Discussion:

Directly observing the influence of climate on species interactions and population dynamics is often challenging because of interacting and nonlinear relationships; here, we

319 directly and quantitatively connect laboratory-based climate relationships to observed
320 mosquito and disease dynamics in the field, supporting the mechanistic role of climate in
321 these disease systems. The trait-based modeling approach helps to reconcile some long-
322 standing inconsistencies in the literature on the effects of climate on arboviral
323 transmission dynamics. Temperature, rainfall, and humidity are commonly correlated
324 with arboviral transmission, but with apparently inconsistent conclusions about which
325 climate variables best predict disease, in what direction, and at what time lags [3–8]. For
326 example, some studies indicate that mean temperature best predicts disease [50–54],
327 while others indicate that minimum temperature [32,45,55,56] or maximum temperature
328 [7,57–59] are better predictors. Rainfall metrics associated with arboviruses vary widely
329 as well, from cumulative rainfall [6,42,53,59] to number of rainy days [60,61] to rainfall
330 rates and thresholds [27,55], and these relationships are difficult to measure in the lab
331 (but see [25]). Further, time lags between climate conditions and dengue incidence are
332 variable rather than static: for example, as temperature and daily rainfall increase, the
333 time lags associated with arboviral incidence decrease [55]. A trait-based model allows
334 these varying time lags to emerge from the nonlinear dynamics of transmission, rather
335 than assuming static time lags. Our results highlight that we should not expect the same
336 climate conditions and lags to be important in all settings, but that their combined,
337 nonlinear effects can predict disease dynamics across different ecological and socio-
338 economic settings.
339
340 Understanding the mechanisms that drive disease dynamics can help address two
341 critically important research priorities: assessing intervention strategies and projecting

342 impacts from climate change on disease dynamics. While phenomenological models
343 often replicate arboviral disease dynamics remarkably well [62], mechanistic models that
344 capture mosquito population dynamics and interactions between mosquitoes and humans
345 will provide more accurate predictions for the effects of different interventions or
346 projected changes in climate. In this study, we assessed intervention efforts and found
347 that efforts to reduce immature mosquito habitat or contact rate between mosquitoes and
348 people should be much more effective than approaches targeted to removing adult
349 mosquitoes. Further, the intervention simulations suggest that even low and moderate
350 intervention intensity (10% and 50% reductions) will result in a large percentage of
351 disease cases averted. These results are promising for supporting integrated disease
352 control efforts for dengue, chikungunya, and Zika. To help policymakers in Kenya
353 interpret how these results can guide local intervention efforts, we created a shiny app
354 based on the SEI-SEIR model (https://jms5151.shinyapps.io/shiny/).
355
356 Comparisons between the model predictions and field observations highlighted several
357 knowledge gaps about climate-disease relationships. While the model generally
358 reproduced patterns of field observations of mosquitoes and disease cases (based on
359 correspondence between z-scores) and observations increased and decreased in unison
360 with the model predictions (based on sign tests), the relative magnitudes only aligned
361 moderately well (based on Pearson's correlations) and there was significant variation
362 across sites (based on Table 1 and ANOVA results) indicating that climate may be a
363 more powerful predictor for differences across a spatial climate gradient (i.e., across
364 sites) than through time within a site, which supports previous findings [63]. Further, we

365 found evidence that rainfall influences transmission dynamics via its effects on mosquito
366 carrying capacity. However, incorporating this effect in a dynamic model requires some
367 knowledge of how humans differentially influence immature mosquito habitat
368 availability across regions. We show support for three hypothesized relationships
369 between rainfall and mosquito carrying capacity in the field, indicating that the
370 relationship between rainfall and immature habitat is highly heterogenous, which has
371 been found in previous research in Ecuador [28] and Kenya [64]. By examining
372 conditions where the SEI-SEIR model systematically under- and overpredicted mosquito
373 abundances and arboviral cases, we identified additional specific climate conditions that
374 warrant further empirical experimentation. In particular, a variety of traits important for
375 transmission are not well understood towards the physiologically relevant limits of
376 temperature [65,66] and humidity [67].
377
378 Future research can build on this study to better predict the location, magnitude, and
379 timing of arboviral outbreaks and to assess additional intervention strategies. This study
380 builds on previous mechanistic and semi-mechanistic models [50,61,68–71] by
381 combining a suite of temperature, rainfall, and humidity dependent trait functions into
382 one epidemiological model. However, there were several factors that we did not include
383 in this study, such as existing vector control programs, gradients in land use and land
384 cover, infrastructure, and preexisting immunity in the population (Table S1). For
385 instance, in Ecuador, factors such as distance to abandoned properties, interruptions in
386 access to piped water, shaded patios, and use of vector control are also known to
387 influence arbovirus transmission [72], whereas in the study sites in Kenya, factors

388 associated with arboviral transmission are less well studied and there are currently no
389 vector control or local arboviral surveillance programs employed. Future studies could
390 further improve the model by incorporating human immune dynamics associated with
391 interactions among different dengue serotypes [73] or cross-reactivity among viral
392 antibodies [74], differential susceptibility across human age classes [75], and
393 heterogeneity in contact rates between mosquitoes and people based on human behavior
394 and movement [50,76]. This study suggests that climate is a key determinant of disease
395 dynamics via its nonlinear effects on mosquito and pathogen traits, and that those
396 relationships can be used to predict the timing and locations of disease outbreaks and to
397 assess intervention strategies. Such mechanistic, climate-driven models will become
398 increasingly important to support public health efforts in the face of novel climate
399 regimes emerging due to climate change.
400
401 **Materials and Methods:**
402 Climate data
403 We collected *in situ* measurements of daily mean temperature, relative humidity, and
404 rainfall at each study site and interpolated missing data where necessary, as described
405 below. We used temperature and humidity measurements from HOBO loggers and
406 rainfall measurements from rain gauges for sites in Kenya. We used temperature,
407 humidity, and rainfall measurements from automatic weather stations operated by the
408 National Institute of Meteorology and Hydrology in Ecuador. For Kenya, we interpolated
409 missing temperature data from NOAA Global Surface Summary of the Day (Table S4,
410 Fig. S2) and interpolated missing rainfall data from NOAA Climate Prediction Center

411 Africa Rainfall Climatology dataset (Table S4, Fig. S3). For Ecuador, we interpolated
412 missing temperature (Table S4, Fig. S2) and rainfall (Table S4, Fig. S3) data using the
413 nearest study site where possible and otherwise based on long term mean values for the
414 corresponding Julian day. To interpolate missing data, we linearly regressed all
415 measurements taken on the same day in two datasets and then used the linear model to
416 interpolate temperature for the site with missing data based on the climate measurement
417 from the secondary source for the date when the data was missing (Fig. S2-3). For
418 rainfall, we first calculated a moving window of 14-day accumulated rainfall (following
419 [77]) for each day before interpolation. For both Kenya and Ecuador, we interpolated
420 missing relative humidity data based on long term mean values for the corresponding
421 Julian day (Table S4). We then calculated the saturation vapor pressure deficit (SVPD)
422 from temperature and humidity to use in the humidity function because previous research
423 suggests SVPD is a more informative measure of the effect of humidity on mosquito
424 survival compared with relative humidity [67]. To calculate SVPD, we first calculated the
425 saturation vapor pressure as:

$$SVP = 610.7 * 10^{7.5*T/(273.3+T)} \quad (1)$$

426 where (T) is temperature in degrees Celsius. We then calculated SVPD (in kilopascals) as

$$SVPD = 1 - \frac{RH}{100} * SVP \quad (2)$$

427 where RH is relative humidity. The final dataset had no missing values for temperature
428 (Fig. S4), rainfall (Fig. S5), and humidity (Fig. S6).
429
430
431

Vector surveys

We collected, counted, sexed, and classified mosquitoes by species, and aggregated the data to mean number of *Aedes aegypti* per house, month, and year to account for differences in survey effort across months and sites. We collected adult mosquitoes using Prokopack aspirators [78]. In Ecuador, we collected mosquitoes from approximately 27 houses per site (range = 3-57 houses across four sites) every one-to-two weeks during three, four-month sampling periods between July 2016 and August 2018 (N = 147 sampling weeks across four sites) to capture different parts of the transmission season. We aggregated the Ecuador vector data to monthly values (N = 60 site-month observations) to correspond with the temporal resolution of surveys in Kenya. In Kenya, we collected mosquitoes from approximately 20 houses per site (range = 1-47 houses across four sites) every month between January 2014 and October 2018 (N = 217 site-month observations). In Kenya, we also collected pupae, late instars, and early instars from containers with standing water around the home and collected eggs by setting ovitraps for an average of four days in and around each house monthly. We brought pupae, late and early instars, and eggs to the insectary and reared them to adulthood to classify individuals by sex and species.

Arboviral surveys

For Ecuador, we analyzed laboratory-confirmed dengue, chikungunya, and Zika cases provided by the Ministry of Health (MoH) of Ecuador. The MoH collects serum samples from a subset of people with suspected arbovirus infections, and samples are tested at the National Public Health Research Institute by molecular diagnostics (RT-PCR) or

455 antibody tests (IgM ELISA for dengue), depending on the number of days of illness.
456 Results are sent to the MoH Epidemiological Surveillance and Control National
457 Directorate (SIVE Alerta system). Laboratory-confirmed dengue cases were available for
458 all four sites from 2014 to 2018. Laboratory-confirmed chikungunya cases were available
459 for Machala and Huaquillas from 2015 to 2018. Laboratory-confirmed Zika cases were
460 available for Machala from 2016 to 2018.
461
462 For Kenya, we used laboratory-confirmed dengue cases aggregated by site and month
463 between 2014 and 2018 collected in a passive surveillance study on childhood febrile
464 illness in Kenya (NIH R01AI102918, PI: ADL). The study population consisted of 7653
465 children less than 18 years of age with undifferentiated febrile illness. Children with fever
466 enrolled in the study when attending outpatient care in one of the four study sites (Mbaka
467 Oromo Health Centre in Chulaimbo, Obama Children's Hospital in Kisumu, Msambweni
468 District Hospital in Msambweni, and Ukunda/Diani Health Center in Ukunda). Local
469 health officers collected comprehensive clinical and demographic data and phlebotomy at
470 the initial visit. We tested each child's blood for dengue viremia by molecular diagnostics
471 (conventional PCR [79] or targeted multiplexed real-time PCR when available [80]), or
472 serologic conversion at a follow up visit (IgG ELISA [81]).
473
474 SEI-SEIR model
475 We adapted an SEI-SEIR model parameterized for dengue transmission in *Ae. aegypti*
476 mosquitoes [82] (Fig. 2) to simulate mosquito abundance and arboviral cases through
477 time based on daily weather conditions in eight study locations. The model (equations 3-

478 9), created independently from the observed data described above, allows mosquito life
479 history traits and viral development rate to vary with temperature (T) following [82],
480 mosquito carrying capacity to vary with accumulated 14-day rainfall (R) following [77],
481 and mosquito mortality to vary with humidity (i.e., saturation vapor pressure deficit) (H)
482 following [67].

$$\frac{dS_m}{dt} = \varphi(T,H) * \frac{1}{\mu(T,H)} * N_m * \left(1 - \frac{N_m}{K(T,R,H)}\right) - \left(a(T) * pMI(T) * \frac{I_h}{N_h} + \mu(T,H)\right) * S_m \quad (3)$$

$$\frac{dE_m}{dt} = a(T) * pMI(T) * \frac{I_h}{N_h} * S_m - \left(PDR(T) + \mu(T,H)\right) * E_m \quad (4)$$

$$\frac{dI_m}{dt} = PDR(T) * E_m - \mu(T,H) * I_m \quad (5)$$

$$\frac{dS_h}{dt} = -a(T) * b(T) * \frac{I_m}{N_h} * S_h + BR * S_h - DR * S_h + ie * N_h - ie * S_h \quad (6)$$

$$\frac{dE_h}{dt} = a(T) * b(T) * \frac{I_m}{N_h} * S_h - \delta * E_h - DR * E_h - ie * E_h \quad (7)$$

$$\frac{dI_h}{dt} = \delta * E_h - \eta * I_h - DR * I_h - ie * I_h \quad (8)$$

$$\frac{dR_h}{dt} = \eta * I_h - DR * R_h - ie * R_h \quad (9)$$

483 where

$$\varphi(T,H) = EFD(T) * pEA(T) * MDR(T) \quad (10)$$

484

485 The mosquito population (N_m) was separated into susceptible (S_m), exposed (E_m), and
486 infectious (I_m) compartments and the human population (N_h) was separated into
487 susceptible (S_h), exposed (E_h), infectious (I_h), and recovered (R_h) compartments (Fig. 2).
488 Climate-independent model parameters (Table 3) included the intrinsic incubation period
489 (δ), human infectivity period (η), birth rate (BR), death rate (DR), and
490 immigration/emigration rate (ie). The temperature-dependent SEI-SEIR model was
491 developed by Huber et al. [82] and allows mosquito life history traits and viral
492 development rates to vary according to thermal response curves fit from data derived in

493 laboratory experiments conducted at constant temperatures (Table 4). The temperature-
494 dependent traits include eggs laid per female per day (EFD), the probability of egg-to-adult
495 survival (pEA), mosquito development rate (MDR), mosquito mortality rate (lifespan^{-1}; μ),
496 biting rate (a), probability of mosquito infection per bite on an infectious host (pMI),
497 parasite development rate (PDR), and probability of mosquito infectiousness given an
498 infectious bite (b). We modified the mosquito mortality rate equation to vary as a function
499 of temperature and humidity by fitting a spline model based on a pooled survival analysis
500 of *Ae. aegypti* [67] (Fig. S7):

$$\mu(T,H) = \frac{1}{c*(T-T_0)*(T-T_m)} + (1-(0.01+2.01*H))*y \qquad H<1 \qquad (11)$$

$$\mu(T,H) = \frac{1}{c*(T-T_0)*(T-T_m)} + (1-(1.22+0.27*H))*y \qquad H\geq 1 \qquad (12)$$

501 where the rate constant (c), minimum temperature (T_0), and maximum temperature (T_m)
502 equal -1.24, 16.63, and 31.85 respectively (Table 4), humidity (H) is the saturation vapor
503 pressure deficit, and y is a scaling factor that we set to 0.005 and 0.01, respectively, to
504 restrict mosquito mortality rates within the range of mortality rates estimated by other
505 studies [20,67]. The linear humidity function has a steeper slope at lower humidity values
506 (equation 11) compared with higher humidity values (equation 12) based on previous
507 research [67] (Fig. S7).
508
509 We modeled mosquito carrying capacity, K, as a modified Arrhenius equation following
510 [82,83]:

$$K(T,H,R) = \frac{EFD(T_0)*pEA(T_0)*MDR(T_0)*\mu(T_0,H_0)^{-1}-\mu(T_0,H_0)}{EFD(T_0)*pEA(T_0)*MDR(T_0)*\mu(T_0,H_0)^{-1}}*N_m \qquad (12)$$
$$*\,e^{\frac{-E_A*(T-T_0)^2}{\kappa_B*(T+273)*(T_0+273)}}*f(R)$$

511 with T_0 and H_0 set to the temperature and humidity where carrying capacity is greatest
512 (29°C and 6 kPA) and the Boltzmann constant, (K_B), is 8.617 x 10^{-5} eV/K. We set the
513 activation energy, E_A, as 0.05 based on [82]. Since there were no experimental data from
514 which to derive the functional response of mosquito carrying capacity across a gradient
515 of rainfall values, we tested several functional relationships based on hypothesized
516 biological relationships between freshwater availability and immature mosquito breeding
517 habitat, modeling the effect of rainfall on carrying capacity, $f(R)$, as either:

$$f(R_{\text{Brière}}) = c * R * (R - R_{min}) * \sqrt{(R_{max} - R)} * y \quad (12)$$

$$f(R_{Quadratic}) = c * (R - R_{min}) * (R - R_{max}) * y \quad (13)$$

$$f(R_{\text{Inverse}}) = \frac{1}{R} \quad (14)$$

518 where minimum rainfall (R_{min}) equaled 1 mm and maximum rainfall (R_{max}) equaled 123
519 mm based on the high probability of flushing [27]. The quadratic function is similar to
520 the rainfall function found in [27] and the inverse function is based on the rainfall
521 function used in [77]. We used rate constants (c) of 7.86e^{-5} and -5.99e^{-3} for the Brière and
522 quadratic functions respectively, based on rate constants for other parameters with similar
523 functional forms (Table 4). We scaled the Brière and quadratic functions by y (0. 268 and
524 0.045, respectively) so that the maximum carrying capacity was approximately equal
525 across all three functions.
526
527
528

Table 3: Values of temperature-invariant parameters used in the model. We derived daily birth and death rates in the model by dividing the per capita birth and death rates by 360 days. The World Bank Open Data can be found at https://data.worldbank.org/.

Parameter	Definition	Value	Source
δ^{-1}	Intrinsic incubation period (days)	5.9	[82]
η^{-1}	Human infectivity period (days)	5.0	[82]
BR	Annual birth rate (per 1000 people)	31.782 (Ecuador) 20.175 (Kenya)	The World Bank Open Data
DR	Annual death rate (per 1000 people)	5.284 (Ecuador) 5.121 (Kenya)	The World Bank Open Data
ie	Immigration/emigration rate	0.01	Expert opinion

Table 4: Fitted thermal responses for *Ae. aegypti* life history traits. Traits were fit to a Brière $[cT(T-T_0)(T_m-T)^{\frac{1}{2}}]$ or a quadratic $[c(T-T_m)(T-T_0)]$ function where T represents temperature. T_0 and T_m are the critical thermal minimum and maximum, respectively, and c is the rate constant. Thermal responses were fit by [20] and also used in [82]. Parasite development rate was measured as the virus extrinsic incubation rate.

Trait	Definition	Function	c	T_0	T_m
a	Biting rate (day^{-1})	Brière	2.71×10^{-04}	14.67	41.00
EFD	Eggs laid per female per day	Brière	2.08×10^{-02}	14.06	32.03
pEA	Probability of mosquito egg-to-adult survival	Quadratic	-3.36×10^{-03}	7.68	38.31
MDR	Mosquito egg-to-adult development rate (day^{-1})	Brière	1.49×10^{-04}	15.12	37.67
Lf	Adult mosquito lifespan (days)	Quadratic	-1.24	16.63	31.85
b	Probability of mosquito infectiousness	Brière	9.86×10^{-04}	12.05	32.79
pMI	Probability of mosquito infection	Brière	5.23×10^{-04}	1.51	34.74
PDR	Parasite development rate (day^{-1})	Brière	1.04×10^{-04}	11.50	38.97

To initiate the model, we used site-specific values for human population size and randomly selected one set of values for all sites for the proportion of mosquitoes and humans in each compartment. For Ecuador, we used population estimates from official population projections produced by Proyección de la Población Ecuatoriana, por años calendario, según cantones 2010-2020 (https://www.ecuadorencifras.gob.ec/proyecciones-poblacionales/) with population sizes of 57,366, 279,887, 13,673, and 25,615 for Huaquillas, Machala, Portovelo, and Zaruma, respectively, based on 2017 projections. For Kenya, we estimated the population sizes

559 served by each outpatient care facility by creating a polygon around all the geolocations
560 of study participants' homes enrolled at each outpatient care facility and summed
561 population count data from NASA's Socioeconomic Data and Applications Center
562 Gridded Population of the World v4 (https://doi.org/10.7927/H4JW8BX5) within each
563 polygon using ArcGIS v 10.4.1. We estimated population sizes of 7,304, 547,557,
564 240,698, and 154,048 for Chulaimbo, Kisumu, Msambweni, and Ukunda respectively.
565 We used the following values as the initial proportion of mosquitoes and humans in each
566 model compartment: S_m = 0.22, E_m = 0.29, I_m = 0.49, S_h = 0.58, E_h = 0.22, I_h = 0.00, and
567 R_h = 0.20. We determined that the model was invariant to initial proportion values after a
568 short burn-in period (90 days) based on a sensitivity analysis (Fig. S8).
569
570 We ran all model simulations using the deSolve package in R statistical software v 3.5.3.
571 Model codes is available at https://github.com/jms5151/SEI-SEIR_Arboviruses.
572
573 Model validation
574 To validate the SEI-SEIR model, we quantified the relationships between predicted and
575 observed mosquitoes and laboratory-confirmed disease cases by comparing z-score
576 values, Pearson's correlations, sign tests, and Analysis of Variance (ANOVAs). To
577 determine whether there was overall correspondence between model predictions and
578 field-collected observations of *Aedes aegypti* abundances (N = 277 site-months) and
579 laboratory-confirmed arboviral incidence (N = 388 site-months), we categorized
580 observations of mosquito abundance or disease cases as corresponding to the model
581 predictions if the observation fell within one standard deviation above or below the

prediction (using z-scores of observations and predictions), overpredicted if the observations were below one standard deviation below the prediction, and underpredicted if the observations were above one standard deviation above the prediction. To assess the correlation of individual survey points through time within sites, we calculated Pearson's correlation coefficient, r, between model predictions of observations using the cor function in base R, excluding missing data. To determine whether the model predicted directional trends in the dynamics, we determined whether model predictions and observations increased and decreased in unison by first calculating the number of time points between surveys where predictions and observations of mosquito abundances or disease cases synchronously increased, decreased, or stayed constant between surveys and then used the number of time points in agreement and the total number of time points in a two-tailed exact sign test using the binom.test function in R. To test whether climate effects were more important for determining differences across sites or whether climate was differentially predictive in some sites over others, we calculated the yearly percentage of mosquito and disease case observations predicted by the model and used those site-year values in a one-way ANOVA using the aov function in R.

CART model

To investigate conditions where the model systematically over- or underpredicted mosquito abundances and arboviral cases, we used classification and regression tree (CART) models. For each CART model, we used the three correspondence categories (corresponded, overpredicted, underpredicted) as the response variable and a suite of predictor variables. The predictor variables included site (proxy for socioeconomic status

and potential prior exposure to disease), country (proxy for genetic, cultural, healthcare, and infrastructure differences), urban/rural, inland/coastal, and climate conditions in the month prior to each survey, a time interval commonly associated with arboviral transmission [6,42,53]. The climate conditions we investigated in the month prior to each survey were minimum, maximum, mean, and variance of daily temperature and humidity and 14-day cumulative rainfall. We conducted the CART analysis using the rpart package in R.

Comparison of R_0 with prior studies

We collected effect sizes of temperature on dengue incidence from 12 peer-reviewed studies from the literature (Table S3). We selected studies with mean temperatures across the predicted temperature range where arboviral transmission can occur. We scaled the coefficient values to visualize the relative effect of temperature across studies given that the original analyses were conducted with different temperature metrics and across different temperature ranges. We provide additional information and sources in Table S3.

Intervention simulations

We simulated different intervention strategies by adapting the SEI-SEIR model and simulating disease cases over a one-year time period. We simulated three intervention strategies (reducing contact rate between mosquitoes and humans, reducing immature mosquito habitat, and reducing mosquito abundance) at three intensity levels (10%, 50%, and 90% reduction). Each of these simulation strategies preserves the temperature-, rainfall-, and humidity-dependence of each parameter but modifies the magnitude of one

628 or more parameters. To simulate a reduction in contact rate, we multiplied the mosquito
629 biting rate, a, by 0.10, 0.50, or 0.90. To simulate a reduction in immature mosquito
630 habitat, we multiplied the carrying capacity function equation, K (equation 12), by 0.10,
631 0.50, or 0.90. To simulate a reduction in mosquito abundance, we reduced the proportion
632 of mosquitoes in the susceptible, exposed, and infectious compartments by 0.10, 0.50, or
633 0.90. In contrast to the first two interventions that are considered relatively "static" (e.g.,
634 adding screens to windows will consistently reduce contact rate), the third intervention
635 represents an activity that is labor intensive and is applied at a single time point (e.g.,
636 spraying insecticide). Therefore, for the third intervention, we ran simulations where the
637 intervention occurred once a year and we varied the timing of the intervention by month
638 (e.g., 12 simulations per intensity level).
639
640 **Acknowledgements:** JMC, ADL, EFL, and EAM were supported by a Stanford Woods
641 Institute for the Environment – Environmental Ventures Program grant (PIs: EAM, ADL,
642 and EFL). EAM was also supported by a Hellman Faculty Fellowship and a Terman
643 Award. ADL, BAN, FMM, ENGS, MSS, ARK, RD, AA, and HNN were supported by a
644 National Institutes of Health R01 grant (AI102918; PI: ADL). EAM, AMSI, and SJR
645 were supported by a National Science Foundation Ecology and Evolution of Infectious
646 Diseases grant (DEB-1518681) and AMSI and SJR were also supported by an NSF DEB
647 RAPID grant (1641145). EAM was supported by a National Institute of General Medical
648 Sciences Maximizing Investigators' Research Award grant (1R35GM133439-01).
649

Author contributions: EAM, ADL, EFL, and JMC conceived of project. JMC conducted analyses and wrote manuscript. EAM, ADL, EFL, and AMSI secured funding for the project. BNN, FMM, EBA, AA, MJBC, RD, FHH, RM, and HNN collected data. ENGS and MMS conducted laboratory analyses. ARK, SJR, and RS processed data. All authors revised and approved of the manuscript.

References:

1. Ockendon N, Baker DJ, Carr JA, White EC, Almond REA, Amano T, et al. Mechanisms underpinning climatic impacts on natural populations: altered species interactions are more important than direct effects. Glob Chang Biol. 2014;20: 2221–2229. doi:10.1111/gcb.12559
2. Boggs CL, Inouye DW. A single climate driver has direct and indirect effects on insect population dynamics. Ecol Lett. 2012;15: 502–508. doi:10.1111/j.1461-0248.2012.01766.x
3. Jury MR. Climate influence on dengue epidemics in Puerto Rico. Int J Environ Health Res. 2008;18: 323–334. doi:10.1080/09603120701849836
4. Campbell KM, Haldeman K, Lehnig C, Munayco C V., Halsey ES, Laguna-Torres VA, et al. Weather Regulates Location, Timing, and Intensity of Dengue Virus Transmission between Humans and Mosquitoes. PLoS Negl Trop Dis. 2015;9: e0003957. doi:10.1371/journal.pntd.0003957
5. Adde A, Roucou P, Mangeas M, Ardillon V, Desenclos J-C, Rousset D, et al. Predicting Dengue Fever Outbreaks in French Guiana Using Climate Indicators. PLoS Negl Trop Dis. 2016;10: e0004681. doi:10.1371/journal.pntd.0004681

673 6. Dhimal M, Gautam I, Joshi HD, O'Hara RB, Ahrens B, Kuch U, et al. Risk
674 Factors for the Presence of Chikungunya and Dengue Vectors (Aedes aegypti and
675 Aedes albopictus), Their Altitudinal Distribution and Climatic Determinants of
676 Their Abundance in Central Nepal. PLoS Negl Trop Dis. 2015;9: e0003545.
677 doi:10.1371/journal.pntd.0003545
678 7. Descloux E, Mangeas M, Menkes CE, Lengaigne M, Leroy A, Tehei T, et al.
679 Climate-Based Models for Understanding and Forecasting Dengue Epidemics.
680 PLoS Negl Trop Dis. 2012;6: e1470. doi:10.1371/journal.pntd.0001470
681 8. Aswi A, Cramb SM, Moraga P, Mengersen K. Epidemiology and Infection
682 Bayesian spatial and spatio-temporal approaches to modelling dengue fever: a
683 systematic review. Epidemiol Infect. 2018;147. doi:10.1017/S0950268818002807
684 9. Hurtado-Daz M, Riojas-Rodrguez H, Rothenberg S, Gomez-Dantes H, Cifuentes
685 E. Impact of climate variability on the incidence of dengue in Mexico. Trop Med
686 Int Heal. 2007;12. doi:10.1111/j.1365-3156.2007.01930.x
687 10. Nakhapakorn K, Tripathi N. An information value based analysis of physical and
688 climatic factors affecting dengue fever and dengue haemorrhagic fever incidence.
689 Int J Health Geogr. 2005;4: 13. doi:10.1186/1476-072X-4-13
690 11. Messina JP, Brady OJ, Scott TW, Zou C, Pigott DM, Duda KA, et al. Global
691 spread of dengue virus types: mapping the 70 year history. Trends Microbiol.
692 2014;22: 138–146. doi:10.1016/j.tim.2013.12.011
693 12. Wilke AB, Beier JC, Benelli G. Complexity of the relationship between global
694 warming and urbanization – an obscure future for predicting increases in vector-
695 borne infectious diseases. Curr Opin Insect Sci. 2019;35: 1–9.

doi:10.1016/J.COIS.2019.06.002

13. Campbell LP, Luther C, Moo-Llanes D, Ramsey JM, Danis-Lozano R, Peterson AT. Climate change influences on global distributions of dengue and chikungunya virus vectors. Philos Trans R Soc B Biol Sci. The Royal Society; 2015;370: 20140135–20140135. doi:10.1098/rstb.2014.0135

14. Messina JP, Brady OJ, Golding N, Kraemer MUG, Wint GRW, Ray SE, et al. The current and future global distribution and population at risk of dengue. Nat Microbiol. 2019; 1. doi:10.1038/s41564-019-0476-8

15. Achee NL, Gould F, Perkins TA, Reiner RC, Morrison AC, Ritchie SA, et al. A Critical Assessment of Vector Control for Dengue Prevention. PLoS Neglected Tropical Diseases. 2015. doi:10.1371/journal.pntd.0003655

16. Michael E, Singh BK, Mayala BK, Smith ME, Hampton S, Nabrzyski J. Continental-scale, data-driven predictive assessment of eliminating the vector-borne disease, lymphatic filariasis, in sub-Saharan Africa by 2020. BMC Med. 2017;15: 176. doi:10.1186/s12916-017-0933-2

17. Smith T, Maire N, Ross A, Penny M, Chitnis N, Schapira A, et al. Towards a comprehensive simulation model of malaria epidemiology and control. Parasitology. 2008. pp. 1507–1516. doi:10.1017/S0031182008000371

18. Kraemer MU, Sinka ME, Duda KA, Mylne AQ, Shearer FM, Barker CM, et al. The global distribution of the arbovirus vectors *Aedes aegypti* and *Ae. albopictus*. Elife. 2015;4. doi:10.7554/eLife.08347

19. Powell JR, Tabachnick WJ, Powell JR, Tabachnick WJ. History of domestication and spread of Aedes aegypti - A Review. Mem Inst Oswaldo Cruz. Fundação

719 Oswaldo Cruz; 2013;108: 11–17. doi:10.1590/0074-0276130395

720 20. Mordecai EA, Cohen JM, Evans M V., Gudapati P, Johnson LR, Lippi CA, et al.
721 Detecting the impact of temperature on transmission of Zika, dengue, and
722 chikungunya using mechanistic models. PLoS Negl Trop Dis. 2017;11: e0005568.
723 doi:10.1371/journal.pntd.0005568

724 21. Shocket MS, Ryan SJ, Mordecai EA. Temperature explains broad patterns of Ross
725 River virus transmission. Elife. 2018; doi:10.7554/eLife.37762.001

726 22. Paull SH, Horton DE, Ashfaq M, Rastogi D, Kramer LD, Diffenbaugh NS, et al.
727 Drought and immunity determine the intensity of West Nile virus epidemics and
728 climate change impacts. Proc R Soc B Biol Sci. 2017;284: 20162078.
729 doi:10.1098/rspb.2016.2078

730 23. Costa EAP de A, Santos EM de M, Correia JC, Albuquerque CMR de. Impact of
731 small variations in temperature and humidity on the reproductive activity and
732 survival of Aedes aegypti (Diptera, Culicidae). Rev Bras Entomol. 2010;54: 488–
733 493. doi:10.1590/S0085-56262010000300021

734 24. Gaaboub IA, El-Sawaf SK, El-Latif MA. Effect of Different Relative Humidities
735 and Temperatures on Egg-Production and Longevity of Adults of Anopheles
736 (Myzomyia) pharoensis Theob.1. Zeitschrift für Angew Entomol. 2009;67: 88–94.
737 doi:10.1111/j.1439-0418.1971.tb02098.x

738 25. Koenraadt CJM, Harrington LC. Flushing Effect of Rain on Container-Inhabiting
739 Mosquitoes Aedes aegypti and Culex pipiens (Diptera: Culicidae). J Med Entomol.
740 2009;45: 28–35. doi:10.1603/0022-2585(2008)45[28:FEOROC]2.0.CO;2

741 26. Paaijmans KP, Wandago MO, Githeko AK, Takken W, Vulule J. Unexpected High

Losses of Anopheles gambiae Larvae Due to Rainfall. PLoS One. 2007;2: e1146. doi:10.1371/journal.pone.0001146

27. Benedum CM, Seidahmed OME, Eltahir EAB, Markuzon N. Statistical modeling of the effect of rainfall flushing on dengue transmission in Singapore. PLoS Negl Trop Dis. 2018;12: e0006935. doi:10.1371/journal.pntd.0006935

28. Stewart Ibarra AM, Ryan SJ, Beltrán E, Mejía R, Silva M, Muñoz Á. Dengue Vector Dynamics (Aedes aegypti) Influenced by Climate and Social Factors in Ecuador: Implications for Targeted Control. PLoS One. 2013;8: e78263. doi:10.1371/journal.pone.0078263

29. Pontes RJ, Spielman A, Oliveira-Lima JW, Hodgson JC, Freeman J. Vector densities that potentiate dengue outbreaks in a Brazilian city. Am J Trop Med Hyg. 2000;62: 378–383. doi:10.4269/ajtmh.2000.62.378

30. Anyamba A, Linthicum KJ, Small JL, Collins KM, Tucker CJ, Pak EW, et al. Climate Teleconnections and Recent Patterns of Human and Animal Disease Outbreaks. PLoS Negl Trop Dis. 2012;6: e1465. doi:10.1371/journal.pntd.0001465

31. Stewart-Ibarra AM, Lowe R. Climate and Non-Climate Drivers of Dengue Epidemics in Southern Coastal Ecuador. Am J Trop Med Hyg. 2013;88: 971–981. doi:10.4269/ajtmh.12-0478

32. Stewart-Ibarra AM, Muñoz ÁG, Ryan SJ, Ayala EB, Borbor-Cordova MJ, Finkelstein JL, et al. Spatiotemporal clustering, climate periodicity, and social-ecological risk factors for dengue during an outbreak in Machala, Ecuador, in 2010. BMC Infect Dis. 2014;14: 610. doi:10.1186/s12879-014-0610-4

33. Agha SB, Tchouassi DP, Turell MJ, Bastos ADS, Sang R. Entomological

765 assessment of dengue virus transmission risk in three urban areas of Kenya. PLoS
766 Negl Trop Dis. 2019;13: e0007686. doi:10.1371/journal.pntd.0007686
767 34. Agha SB, Tchouassi DP, Bastos ADS, Sang R. Dengue and yellow fever virus
768 vectors: seasonal abundance, diversity and resting preferences in three Kenyan
769 cities. Parasit Vectors. 2017;10: 628. doi:10.1186/s13071-017-2598-2
770 35. Chretien J-P, Anyamba A, Bedno SA, Breiman RF, Sang R, Sergon K, et al.
771 Drought-Associated Chikungunya Emergence Along Coastal East Africa. Am J
772 Trop Med Hyg. 2007;76: 405–407. doi:10.4269/ajtmh.2007.76.405
773 36. Hortion J, Mutuku FM, Eyherabide AL, Vu DM, Boothroyd DB, Grossi-Soyster
774 EN, et al. Acute Flavivirus and Alphavirus Infections among Children in Two
775 Different Areas of Kenya, 2015. Am J Trop Med Hyg. 2019;100: 170–173.
776 doi:10.4269/ajtmh.18-0297
777 37. Vu DM, Mutai N, Heath CJ, Vulule JM, Mutuku FM, Ndenga BA, et al.
778 Unrecognized Dengue Virus Infections in Children, Western Kenya, 2014-2015.
779 Emerg Infect Dis. 2017;23: 1915–1917. doi:10.3201/eid2311.170807
780 38. Gubler DJ, Nalim S, Saroso JS, Saipan H, Tan R. Variation in Susceptibility to
781 Oral Infection with Dengue Viruses among Geographic Strains of Aedes Aegypti
782 *. Am J Trop Med Hyg. 1979;28: 1045–1052. doi:10.4269/ajtmh.1979.28.1045
783 39. Xavier-Carvalho C, Chester Cardoso C, de Souza Kehdya F, Guilherme Pacheco
784 A, Ozório Moraesa M. Host genetics and dengue fever. Infect Genet Evol.
785 2017;56: 99–110. doi:10.1016/J.MEEGID.2017.11.009
786 40. Sriprom M, Chalvet-Monfray K, Chaimane T, Vongsawat K, Bicout DJ. Monthly
787 district level risk of dengue occurrences in Sakon Nakhon Province, Thailand. Sci

Total Environ. 2010;408: 5521–5528. doi:10.1016/J.SCITOTENV.2010.08.024

41. Martínez-Bello D, López-Quílez A, Prieto AT. Spatiotemporal modeling of relative risk of dengue disease in Colombia. Stoch Environ Res Risk Assess. 2018;32: 1587–1601. doi:10.1007/s00477-017-1461-5

42. Colón-González FJ, Bentham G, Lake IR. Climate Variability and Dengue Fever in Warm and Humid Mexico. Am J Trop Med Hyg. 2011;84: 757–763. doi:10.4269/ajtmh.2011.10-0609

43. Wang C, Jiang B, Fan J, Wang F, Liu Q. A Study of the Dengue Epidemic and Meteorological Factors in Guangzhou, China, by Using a Zero-Inflated Poisson Regression Model. Asia Pacific J Public Heal. 2014;26: 48–57. doi:10.1177/1010539513490195

44. Minh An DT, Rocklöv J. Epidemiology of dengue fever in Hanoi from 2002 to 2010 and its meteorological determinants. Glob Health Action. 2014;7: 23074. doi:10.3402/gha.v7.23074

45. Laureano-Rosario AE, Garcia-Rejon JE, Gomez-Carro S, Farfan-Ale JA, Muller-Kargera FE. Modelling dengue fever risk in the State of Yucatan, Mexico using regional-scale satellite-derived sea surface temperature. Acta Trop. 2017;172: 50–57. doi:10.1016/j.actatropica.2017.04.017

46. Wu P-C, Guoa H-R, Lung S-C, Lin C-Y, Su H-J. Weather as an effective predictor for occurrence of dengue fever in Taiwan. Acta Trop. 2007;103: 50–57. doi:10.1016/j.actatropica.2007.05.014

47. Karim MN, Munshi SU, Anwar N, Alam MS. Climatic factors influencing dengue cases in Dhaka city: a model for dengue prediction. Indian J Med Res. 2012;136:

811 32–9. Available: http://www.ncbi.nlm.nih.gov/pubmed/22885261

812 48. Gharbi M, Quenel P, Gustave J, Cassadou S, Ruche G La, Girdary L, et al. Time
813 series analysis of dengue incidence in Guadeloupe, French West Indies:
814 Forecasting models using climate variables as predictors. BMC Infect Dis.
815 2011;11: 166. doi:10.1186/1471-2334-11-166

816 49. Sharmin S, Glass K, Viennet E, Harley D. Interaction of Mean Temperature and
817 Daily Fluctuation Influences Dengue Incidence in Dhaka, Bangladesh. PLoS Negl
818 Trop Dis. 2015;9: e0003901. doi:10.1371/journal.pntd.0003901

819 50. Wesolowski A, Qureshi T, Boni MF, Sundsøy PR, Johansson MA, Rasheed SB, et
820 al. Impact of human mobility on the emergence of dengue epidemics in Pakistan.
821 Proc Natl Acad Sci. National Academy of Sciences; 2015;112: 11887–11892.
822 doi:10.1073/pnas.1504964112

823 51. Morin CW, Monaghan AJ, Hayden MH, Barrera R, Ernst K. Meteorologically
824 Driven Simulations of Dengue Epidemics in San Juan, PR. PLoS Negl Trop Dis.
825 2015;9: e0004002. doi:10.1371/journal.pntd.0004002

826 52. Chowell G, Cazelles B, Broutin H, Munayco C V. The influence of geographic
827 and climate factors on the timing of dengue epidemics in Perú, 1994-2008. BMC
828 Infect Dis. 2011;11: 164. doi:10.1186/1471-2334-11-164

829 53. Johansson MA, Dominici F, Glass GE. Local and Global Effects of Climate on
830 Dengue Transmission in Puerto Rico. PLoS Negl Trop Dis. 2009;3: e382.
831 doi:10.1371/journal.pntd.0000382

832 54. Earnest A, Tan SB, Wilder-Smith A. Meteorological factors and El Niño Southern
833 Oscillation are independently associated with dengue infections. Epidemiol Infect.

2012;140: 1244–1251. doi:10.1017/s095026881100183x

55. Chien L-C, Yu H-L. Impact of meteorological factors on the spatiotemporal patterns of dengue fever incidence. Environ Int. Pergamon; 2014;73: 46–56. doi:10.1016/J.ENVINT.2014.06.018

56. Wijayanti SPM, Porphyre T, Chase-Topping M, Rainey SM, McFarlane M, Schnettler E, et al. The Importance of Socio-Economic Versus Environmental Risk Factors for Reported Dengue Cases in Java, Indonesia. PLoS Negl Trop Dis. 2016;10: e0004964. doi:10.1371/journal.pntd.0004964

57. Hu W, Clements A, Williams G, Tong S. Dengue fever and El Nino/Southern Oscillation in Queensland, Australia: a time series predictive model. Occup Environ Med. 2010;67: 307–11. doi:10.1136/oem.2008.044966

58. Chen S-C, Hsieha M-H. Modeling the transmission dynamics of dengue fever: Implications of temperature effects. Sci Total Environ. 2012;431: 385–391. doi:10.1016/J.SCITOTENV.2012.05.012

59. Pinto E, Coelho M, Oliver L, Massad E. The influence of climate variables on dengue in Singapore. Int J Environ Health Res. 2011;21: 415–426. doi:10.1080/09603123.2011.572279

60. Xu L, Stige LC, Chan K-S, Zhou J, Yang J, Sang S, et al. Climate variation drives dengue dynamics. Proc Natl Acad Sci U S A. 2017;114: 113–118. doi:10.1073/pnas.1618558114

61. Li R, Xu L, Bjørnstad ON, Liu K, Song T, Chen A, et al. Climate-driven variation in mosquito density predicts the spatiotemporal dynamics of dengue. Proc Natl Acad Sci. 2019;119: 3624–3629. doi:10.1073/PNAS.1806094116

857 62. Johansson MA, Apfeldorf KM, Dobson S, Devita J, Buczak AL, Baugher B, et al.
858 An open challenge to advance probabilistic forecasting for dengue epidemics. Proc
859 Natl Acad Sci. 2019; 201909865. doi:10.1073/pnas.1909865116
860 63. Harris M, Caldwell JM, Mordecai EA. Climate drives spatial variation in Zika
861 epidemics in Latin America. Proc R Soc B Biol Sci. 2019;286.
862 doi:10.1098/rspb.2019.1578
863 64. Ngugi HN, Mutuku FM, Ndenga BA, Musunzaji PS, Mbakaya JO, Aswani P, et al.
864 Characterization and productivity profiles of Aedes aegypti (L.) breeding habitats
865 across rural and urban landscapes in western and coastal Kenya. Parasit Vectors.
866 2017;10: 331. doi:10.1186/s13071-017-2271-9
867 65. Waite JL, Suh E, Lynch PA, Thomas MB. Exploring the lower thermal limits for
868 development of the human malaria parasite, *Plasmodium falciparum*. Biol Lett.
869 2019;15: 20190275. doi:10.1098/rsbl.2019.0275
870 66. Mordecai EA, Caldwell JM, Grossman MK, Lippi CA, Johnson LR, Neira M, et
871 al. Thermal biology of mosquito-borne disease. Byers J (Jeb), editor. Ecol Lett.
872 2019; ele.13335. doi:10.1111/ele.13335
873 67. Schmidt CA, Comeau G, Monaghan AJ, Williamson DJ, Ernst KC. Effects of
874 desiccation stress on adult female longevity in Aedes aegypti and Ae. albopictus
875 (Diptera: Culicidae): results of a systematic review and pooled survival analysis.
876 Parasit Vectors. 2018;11: 267. doi:10.1186/s13071-018-2808-6
877 68. Wang X, Tang S, Cheke RA. A stage structured mosquito model incorporating
878 effects of precipitation and daily temperature fluctuations. J Theor Biol. 2016;411:
879 27–36. doi:10.1016/j.jtbi.2016.09.015

880 69. Yang HM, Macoris MLG, Galvani KC, Andrighetti MTM, Wanderley DM V.
881 Assessing the effects of temperature on the population of *Aedes aegypti* , the
882 vector of dengue. Epidemiol Infect. 2009;137: 1188–1202.
883 doi:10.1017/S0950268809002040
884 70. Siraj AS, Oidtman RJ, Huber JH, Kraemer MUG, Brady OJ, Johansson MA, et al.
885 Temperature modulates dengue virus epidemic growth rates through its effects on
886 reproduction numbers and generation intervals. PLoS Negl Trop Dis. 2017;11:
887 e0005797. doi:10.1371/journal.pntd.0005797
888 71. Oidtman RJ, Lai S, Huang Z, Yang J, Siraj AS, Reiner RC, et al. Inter-annual
889 variation in seasonal dengue epidemics driven by multiple interacting factors in
890 Guangzhou, China. Nat Commun. 2019;10. doi:10.1038/s41467-019-09035-x
891 72. Kenneson A, Beltrán-Ayala E, Borbor-Cordova MJ, Polhemus ME, Ryan SJ, Endy
892 TP, et al. Social-ecological factors and preventive actions decrease the risk of
893 dengue infection at the household-level: Results from a prospective dengue
894 surveillance study in Machala, Ecuador. PLoS Negl Trop Dis. 2017;11: e0006150.
895 doi:10.1371/journal.pntd.0006150
896 73. Reich NG, Shrestha S, King AA, Rohani P, Lessler J, Kalayanarooj S, et al.
897 Interactions between serotypes of dengue highlight epidemiological impact of
898 cross-immunity. J R Soc Interface. 2013;10: 20130414.
899 doi:10.1098/rsif.2013.0414
900 74. Wen J, Elong Ngono A, Regla-Nava JA, Kim K, Gorman MJ, Diamond MS, et al.
901 Dengue virus-reactive CD8+ T cells mediate cross-protection against subsequent
902 Zika virus challenge. Nat Commun. 2017;8: 1459. doi:10.1038/s41467-017-

01669-z

75. Rodriguez-Barraquer I, Salje H, Cummings DA. Opportunities for improved surveillance and control of dengue from age-specific case data. Elife. 2019;8. doi:10.7554/eLife.45474

76. Stoddard ST, Forshey BM, Morrison AC, Paz-Soldan VA, Vazquez-Prokopec GM, Astete H, et al. House-to-house human movement drives dengue virus transmission. Proc Natl Acad Sci 2013;110: 994–999. doi:10.1073/pnas.1213349110

77. Vaidya A, Bravo-Salgado AD, Mikler AR. Modeling climate-dependent population dynamics of mosquitoes to guide public health policies. Proc 5th ACM Conf Bioinformatics 2014; 380–389. doi:10.1145/2649387.2649415

78. Vazquez-Prokopec GM, Galvin WA, Kelly R, Kitron U. A New, Cost-Effective, Battery-Powered Aspirator for Adult Mosquito Collections. J Med Entomol. 2009;46: 1256–1259. doi:10.1603/033.046.0602

79. Waggoner JJ, Gresh L, Mohamed-Hadley A, Ballesteros G, Davila MJV, Tellez Y, et al. Single-Reaction Multiplex Reverse Transcription PCR for Detection of Zika, Chikungunya, and Dengue Viruses. Emerg Infect Dis. 2016;22: 1295–7. doi:10.3201/eid2207.160326

80. Lanciotti RS, Calisher CH, Gubler DJ, Chang GJ, Vorndam A V. Rapid detection and typing of dengue viruses from clinical samples by using reverse transcriptase-polymerase chain reaction. J Clin Microbiol. 1992;30: 545–51. Available: http://www.ncbi.nlm.nih.gov/pubmed/1372617

81. Grossi-Soyster EN, Cook EAJ, de Glanville WA, Thomas LF, Krystosik AR, Lee

926 J, et al. Serological and spatial analysis of alphavirus and flavivirus prevalence and
927 risk factors in a rural community in western Kenya. PLoS Negl Trop Dis. 2017;11:
928 e0005998. doi:10.1371/journal.pntd.0005998
929 82. Huber JH, Childs ML, Caldwell JM, Mordecai EA. Seasonal temperature variation
930 influences climate suitability for dengue, chikungunya, and Zika transmission.
931 PLoS Negl Trop Dis. 2018;12: e0006451. doi:10.1371/journal.pntd.0006451
932 83. Palamara GM, Childs DZ, Clements CF, Petchey OL, Plebani M, Smith MJ.
933 Inferring the temperature dependence of population parameters: The effects of
934 experimental design and inference algorithm. Ecol Evol. 2014;4: 4736–4750.
935 doi:10.1002/ece3.1309
936